

# Final Report for YSU Center of Transportation and Materials Engineering (YSU CTME)

**Project Title:**

Fabrication and Testing of Low-  
Temperature Catalytically Active  
Washcoat Materials for Next-  
Generation Vehicle Catalytic Converters

**Prepared by:**

Ruigang Wang (PI)  
Department of Chemistry  
Youngstown State University

## DISCLAIMER

*The content of this report reflect the views of the authors, who are Responsible for the facts and the accuracy of the information presented herein. This document is disseminated under the sponsorship of the Department of Transportation University Transportation Centers Program, in the interest of information exchange. The U.S. Government assumes no liability for the Contents or use thereof.*

**1/6/2014**

**Summary:** With funds from this grant, Youngstown State University has purchased a Quantachrome iQ Chemisorption Analyzer and built a Chemical Reactor with Gas Chromatographer for catalyst characterization. PI has been involved in the purchase and installation of the instruments. The two new instruments were fully operational in the spring of 2013 and have so far been used for student research. For the research projects, we found that the nucleation and oxidation of  $\text{Ce}(\text{OH})_3$  are critical steps which needs careful control in order to synthesize different morphological  $\text{CeO}_2$  nanocrystals. The combination of stirring and oxidation of suspension could destroy the nucleation and growth of  $\text{Ce}(\text{OH})_3$ , resulting in the formation of irregular  $\text{CeO}_2$  nanocrystals during the hydrothermal reactions. We demonstrated a general route for shape-controlled synthesis of  $\text{CeO}_2$  nanocrystals via mediation of the  $\text{Ce}(\text{OH})_3$  seed before hydrothermal reactions. It was revealed that the shape of  $\text{CeO}_2$  support plays a critical role in metal- $\text{CeO}_2$  catalytic activity for low-temperature CO oxidation. Out of this project, six refereed and four proceeding papers were published, along with several oral presentations made by PI and students.

### Student Researchers Involved in This Grant:

Name (s)	Affiliation	Job Description
Samuel Mutinda (PhD graduate)	YSU, Chemistry	Catalytic activity and TEM characterization
Varun Sama (MS graduate)	YSU, Chemistry	Surface analysis of materials and heterogeneous catalysts
Aron Korir (Undergraduate)	YSU, Chemistry and Forensic Science	solution based oxide nanomaterials synthesis and characterization
Randi Dangerfield (Undergraduate)	YSU, Chemistry	solution based oxide nanomaterials synthesis and characterization
Zach Brown (Undergraduate)	YSU, Chemistry	solution based oxide nanomaterials synthesis and characterization

## 1. Instrument Acquisition

Acquisition of the state-of-the-art Quantachrome iQ Chemisorption Analyzer and Building a Chemical Reactor with Gas Chromatographer, shown in Figure 1, benefit our program not only by providing new research capabilities currently unavailable to us, but also in student learning and courses/labs. Because of our strong "hands-on" access policy regarding graduate and undergraduate access to *all* research-grade equipment in our department, our students are the primary beneficiaries of these acquisitions.

Temperature programmed reduction (TPR) is a technique for the characterization of solid materials and is often used in the area of heterogeneous catalysis to establish the most efficient reduction conditions [Washes 1996, Datye 1988, Flytzani-Stephanopoulos 2012, Gorte 2010, Cuenya 2010]. In this project, we used CO-TPR to characterize redox properties and CO consumption of CeO<sub>2</sub> during reduction, which are directly related to catalytic activity. QuantaChrome iQ performs the following functions on a fully automated basis: temperature programmed reduction; temperature programmed oxidation; temperature programmed desorption; pulse chemisorption and BET surface area measurements.



Figure 1. Quantachrome iQ Chemisorption Analyzers for BET surface area and catalytic activity measurements of materials.

The catalytic oxidation of CO was conducted by using a fixed bed plug flow reactor system, shown in Figure 2, which was built in this project. 1vol%CO/20vol%O<sub>2</sub>/79vol%He with a 70 mL/min flow rate is supplied through mass flow controller and passed through the catalyst bed. The catalyst (~100 mg) is mixed with quartz wool and filled in the quartz tube reactor. The reaction temperature is programmed between room temperature and 300°C and monitored by thermocouple. The reactant CO and product CO<sub>2</sub> is analyzed by using an on-line gas chromatograph (SRI multiple gas analyzer GC, 8610C) system.

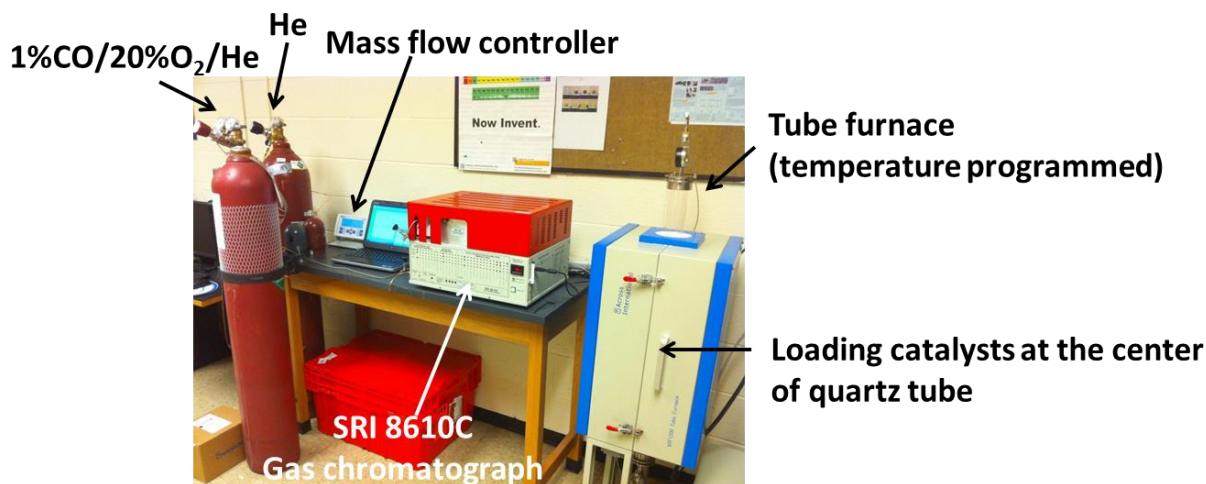
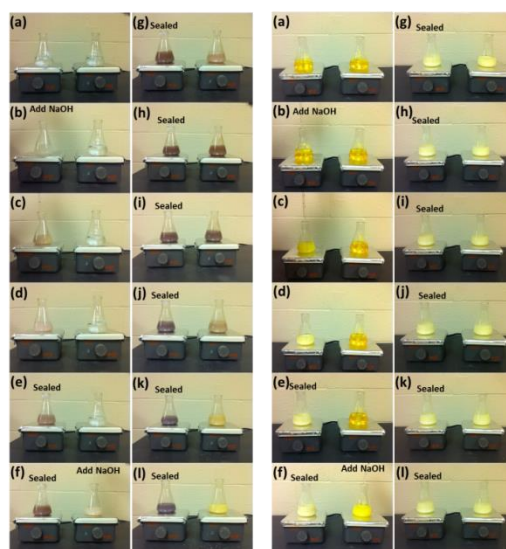


Figure 2. A chemical reactor with residual gas analyzer for measuring CO conversion.

## 2. Major Accomplishments

### *Seed-mediated synthesis of shape-controlled CeO<sub>2</sub> nanocrystals*

**Origin of the color change.** When using trivalent cerium precursor (Ce(NO<sub>3</sub>)<sub>3</sub>), the expected Ce(OH)<sub>3</sub> precipitate was unstable in air at even room temperature, and the final product showed a yellow color originated from lilac after 20 min stirring. This indicates the occurrence of oxidation of the sample as only CeO<sub>2</sub> or Ce(OH)<sub>4</sub> with tetravalent Ce<sup>4+</sup> possess yellow color [Yuan 2009 and Lin 2010]. In order to understand the origin of the color change, two comparison experiments were performed.

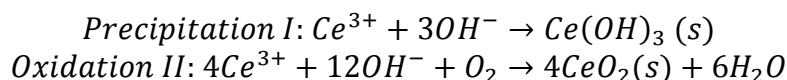


(i) Ce(NO<sub>3</sub>)<sub>3</sub>    (ii) Ce(NH<sub>4</sub>)<sub>2</sub>(NO<sub>3</sub>)<sub>6</sub>

Figure 3. The color change of the precipitate suspension for the sealed and unsealed samples with continuous stirring for a mixture of 6 M NaOH solution with different cerium precursors

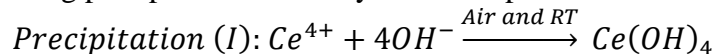
((i)  $Ce(NO_3)_3$ , (ii)  $Ce(NH_4)_2(NO_3)_6$ ). The left flask was sealed and the right one was not sealed after NaOH addition during the 20 min stirring.

In comparison experiment 1, two conical flasks both with 88 mL 0.1 M  $Ce(NO_3)_3$  and a stir bar were put on two magnetic hot plates, and then the solutions were stirred as 8 mL 6M NaOH solution was added to each flask. For the first flask, after adding NaOH, the flask was sealed with Parafilm, and the second flask was left unsealed (exposed to air) after adding NaOH. In comparison experiment 2, everything was set up the same as in experiment 1 except using 0.1 M  $(NH_4)_2Ce(NO_3)_6$  instead of 0.1 M  $Ce(NO_3)_3$  as the starting cerium precursor. Figure 3 shows the results for these two comparison experiments. In experiment 1 using  $Ce(NO_3)_3$ , the unsealed sample showed the color change from lilac to dark gray and then to yellow after 20 min stirring. However, the sealed sample did not show the same color change, and the final suspension still presented a dark gray color. The only difference between these two suspensions in the flasks, shown in Figure 3, was the accessibility of air (oxygen) to the suspension solution, so the color change to yellow for the unsealed sample clearly indicates an occurrence of oxidation during the stirring. A possible explanation for the color change when using trivalent cerium precursor  $Ce(NO_3)_3$  such as in Figure 3 i, could be as follows, involving a precipitation step (I) of the cerium precursor, followed by a dehydration/oxidation step (II):



The actual occurrence of these two reactions depends on the availability of the dissolved oxygen in the solution and oxygen at the air/liquid interface.  $Ce(OH)_3$  nuclei form as soon as  $Ce^{3+}$  ions are mixed with NaOH solution.  $Ce(OH)_3$  is not stable in air, and thus when vigorously stirring the solution in air,  $Ce(OH)_3$  can react with oxygen and then become oxidized to  $CeO_2$ . The role of stirring may relate to the kinetics of oxygen/ $Ce(OH)_3$  gas-solid interaction, thus favoring the formation of  $CeO_2$  by introduction of stirring. For the unsealed sample, both steps I and II can proceed completely resulting in the formation of yellow  $CeO_2$ , while for the sealed sample, the availability of oxygen was limited, so only a relatively small quantity of  $Ce(OH)_3$  can be transformed to  $CeO_2$ , leading to no color change after about 6 min during stirring.

The comparison experiment 2 further clarified the effect of oxidation of  $Ce(OH)_3$  during stirring treatment, by using tetravalent cerium precursor 0.1 M  $Ce(NH_4)_2(NO_3)_6$  as the starting material. As Ce ion possesses +4 valence state in  $Ce(NH_4)_2(NO_3)_6$ , the addition of 6 M NaOH to the  $Ce(NH_4)_2(NO_3)_6$  solution results in a precipitation reaction to form  $Ce(OH)_4$  (yellow color). When the cerium source was changed from  $Ce(NO_3)_3$  to  $Ce(NH_4)_2(NO_3)_6$ , a soluble source of Ce(IV), no such color change was observed as shown in Figure 3 ii, except in the early stage of reaction (0 to ~3 minutes of stirring). This early color change could be due to the formation of  $Ce(OH)_4$  from  $Ce(NH_4)_2(NO_3)_6$ . After this initial period, the color of the precipitate suspension remained unchanged, even after dehydration of  $Ce(OH)_4$  to  $CeO_2$  because no change of oxidation state was involved in the process. A possible mechanism for the observation shown in Figure 3 ii may involve the following precipitation and dehydration steps:



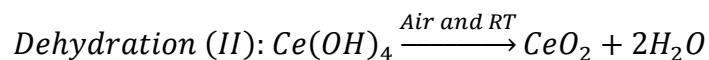


**Table 1** Crystalline size of CeO<sub>2</sub> nanocrystals

Cerium precursor	Sealed	Unsealed
Ce <sup>3+</sup> : Ce(NO <sub>3</sub> ) <sub>3</sub>	7.3 nm	3.4 nm
Ce <sup>4+</sup> : Ce(NH <sub>4</sub> ) <sub>2</sub> (NO <sub>3</sub> ) <sub>6</sub>	2.8 nm	2.8 nm

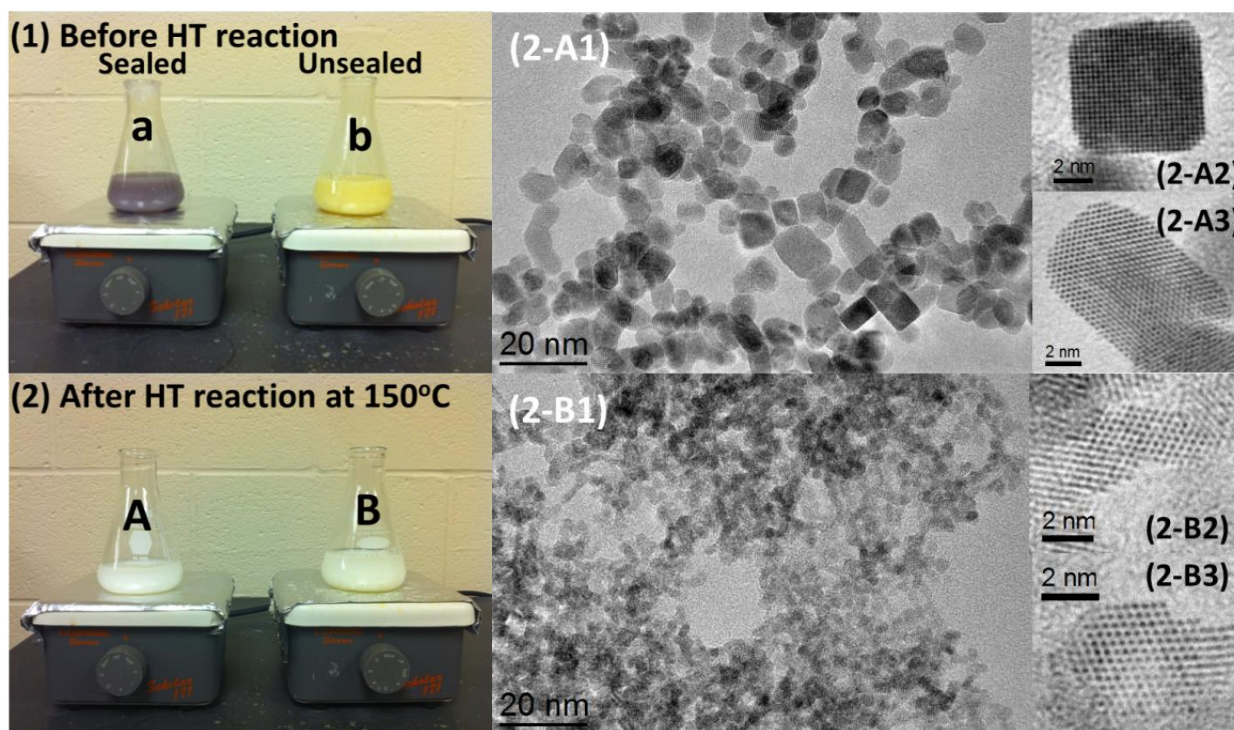


Figure 4. A comparison of color difference and corresponding TEM images between the sealed and unsealed suspension solutions using Ce(NO<sub>3</sub>)<sub>3</sub> before and after hydrothermal reaction. Both of the samples were stirred for 20 min. Sample a/A was sealed during the stirring, while sample b/B was not.

Figure 4 compares the color difference of the suspension solutions between the sealed and unsealed samples using Ce(NO<sub>3</sub>)<sub>3</sub> before and after the hydrothermal reactions at 150°C for 48 hrs. After the hydrothermal reactions, both of the samples show white color, but high resolution TEM (HRTEM) images show that the nanoparticles for the unsealed sample have an irregular shape with a size of 3~4 nm, while most of the nanoparticles for the sealed sample display nanocubes/nanocuboids with a size of 6~10 nm. The sealed sample using Ce(NO<sub>3</sub>)<sub>3</sub> presents the best crystallinity and largest particle size. The diffractogram pattern taken from HRTEM images from individual cerium oxide nanocubes/nanocuboids reveals the single crystal nature of the cubes with {100} facets.

**Shape-controlled hydrothermal synthesis of CeO<sub>2</sub> nanocrystals.** It is commonly assumed that continuous stirring will lead to a more thorough dispersion of newly formed nuclei during the precipitation reaction and result in more compositionally homogeneous products. The observation above demonstrated that the formation (and/or shape/size) of Ce(OH)<sub>3</sub> crystal seeds play a critical role in synthesizing shape/size-controlled CeO<sub>2</sub> nanocrystals. Based on this strategy, we prepared CeO<sub>2</sub> nanocrystals of different morphology at different temperatures and dwell times, in which the Ce(NO<sub>3</sub>)<sub>3</sub>/ NaOH suspension solutions were not stirred and quickly transferred to autoclaves for the hydrothermal reactions at different temperatures and dwell times. Figure 5 shows representative TEM images of CeO<sub>2</sub> nanocrystals with controlled morphology. Table 2 displays the crystalline size calculated using (111) diffraction peaks in the powder XRD patterns and the BET surface area of CeO<sub>2</sub> nanocrystals prepared by different hydrothermal reaction temperature and dwell time. The well-dispersed CeO<sub>2</sub> nanocrystals with different shapes and sizes including nanosheets, nanorods, nanocubes, and nanocuboids can be obtained by the control of reaction temperature and dwell time. In general, the CeO<sub>2</sub> nanocrystals seemed to prefer the morphology of nanosheets and nanorods at low-temperature ( $\leq 130^\circ\text{C}$ ) hydrothermal conditions, while at higher temperature the nanocube-like or irregular shapes were observed.

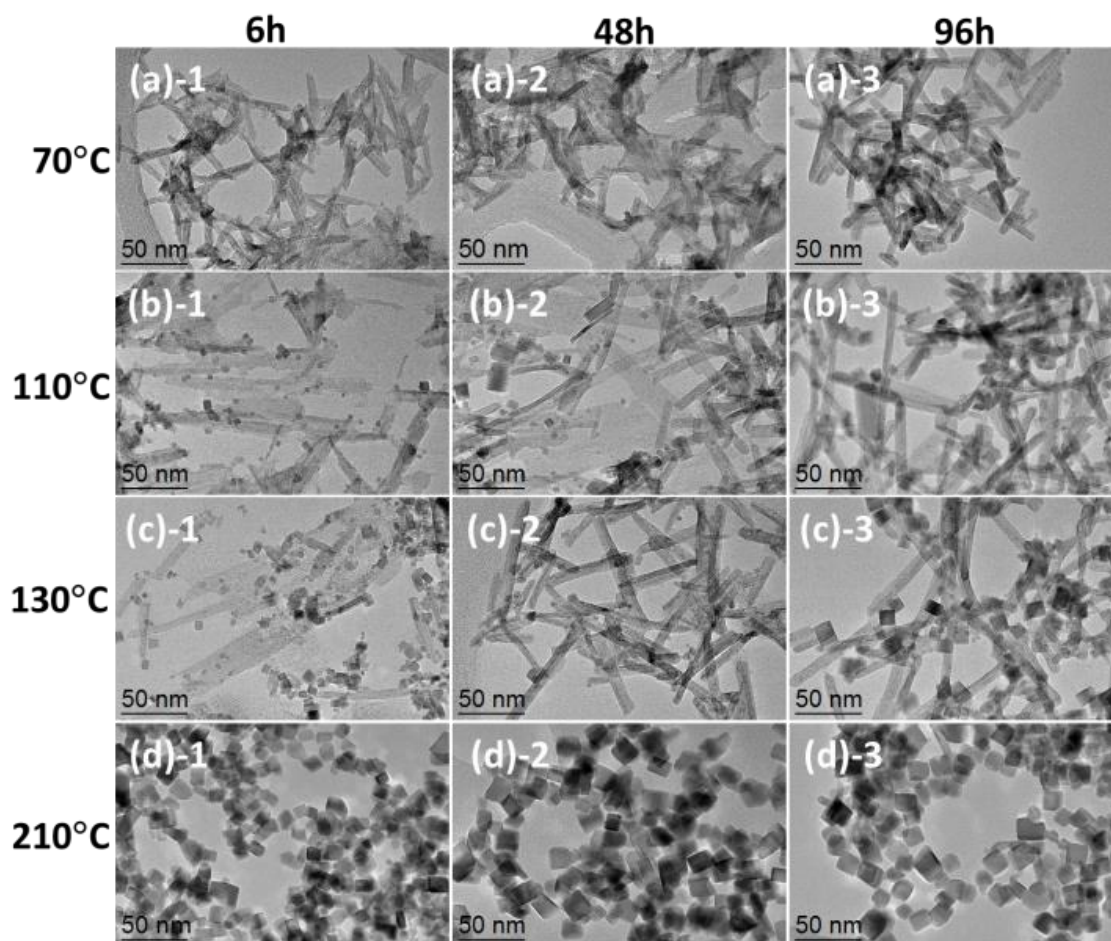


Figure 5. TEM images of CeO<sub>2</sub> nanocrystals prepared by a hydrothermal method at different temperatures (a: 70°C; b: 110°C; c: 130°C; d: 210°C) and dwell time (1: 6h; 2: 48h; 3: 96h).

**Table 2** Crystalline size and BET surface area of CeO<sub>2</sub> nanocrystals prepared by different hydrothermal reaction temperature and dwell time

	6 h		48 h		96 h	
	Crystalline size (nm)	BET surface area (m <sup>2</sup> /g)	Crystalline size (nm)	BET surface area (m <sup>2</sup> /g)	Crystalline size (nm)	BET surface area (m <sup>2</sup> /g)
<b>70°C</b>	4.1	77	4.3	76	5.0	69
<b>110°C</b>	5.3	78	7.3	70	14.1	68
<b>130°C</b>	5.3	71	11.4	65	15.2	52
<b>210°C</b>	17.7	47	17.7	46	17.0	52

According to the results above, Figure 6 shows a schematic diagram, which summarizes the shape-controlled synthesis strategy of CeO<sub>2</sub> nanocrystals in this study. The synthesis mechanisms may be described as follows. A precipitate is obtained by adding NaOH to Ce(NO<sub>3</sub>)<sub>3</sub> or Ce(NH<sub>4</sub>)<sub>2</sub>(NO<sub>3</sub>)<sub>6</sub>. If using Ce(NH<sub>4</sub>)<sub>2</sub>(NO<sub>3</sub>)<sub>6</sub> as cerium precursor, the formation of Ce(OH)<sub>4</sub> and subsequent decomposition to CeO<sub>2</sub> leads to the growth of irregular nanocrystals during hydrothermal reactions. If using Ce(NO<sub>3</sub>)<sub>3</sub> as cerium precursor, the oxidation (to Ce(OH)<sub>4</sub> or CeO<sub>2</sub>) or disturbance of Ce(OH)<sub>3</sub> nucleation also results in formation of irregular CeO<sub>2</sub> nanocrystals during hydrothermal reactions. Shape-controlled CeO<sub>2</sub> nanorods and nanocubes can be only obtained by fast mild stirring or without stirring treatment to avoid oxidation of Ce(OH)<sub>3</sub> before sealing the mixture of NaOH and Ce(NO<sub>3</sub>)<sub>3</sub> for hydrothermal reaction. Therefore, the controllable formation of Ce(OH)<sub>3</sub> from solution seems to be a key to growing different morphological CeO<sub>2</sub> nanocrystals, although the synthetic mechanism of CeO<sub>2</sub> nanosheets, nanorods, and nanocubes obtained during the hydrothermal reaction is still not well understood and needs further investigation.

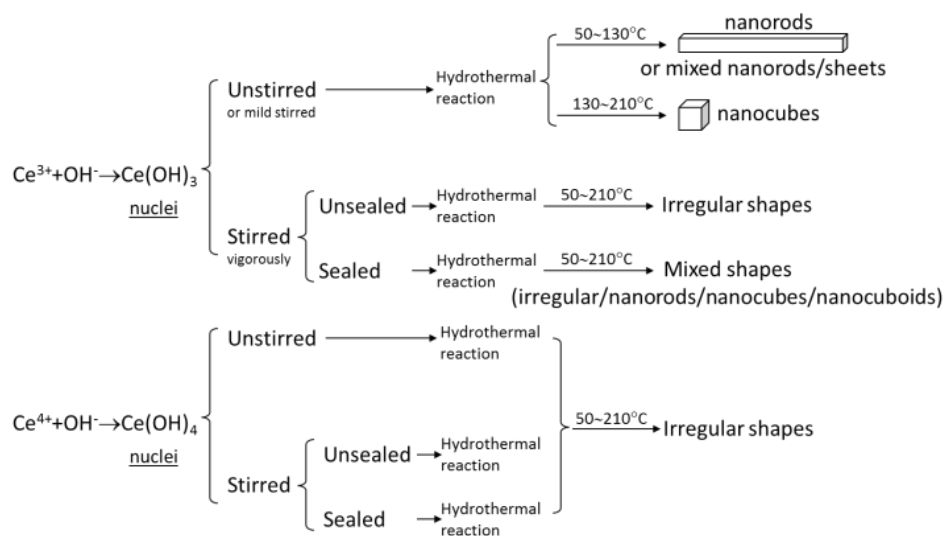


Figure 6. Schematic diagram showing the shape-controlled synthesis of CeO<sub>2</sub> nanocrystals

## Shape Effect on CO Oxidation for Noble or Transition Metal-Loaded CeO<sub>2</sub>: Chemisorption and Catalytic Activity Studies

Experimentally, very little is known for the shape effect of CeO<sub>2</sub> support in metal-CeO<sub>2</sub> catalysts for CO oxidation, particularly for comparing the shape effect on different metal nanoparticles (noble vs. transition metals). A careful investigation of the metal-CeO<sub>2</sub> support with different crystallographic surfaces through structural and catalytic activity studies may provide further mechanistic insights about low temperature CO oxidation. In this research objective, we aim to understand of the role of CeO<sub>2</sub> support in the shape of nanorods, nanotubes, or nanocubes with reactive {200}, {110}, {211} faces on the crystal surface on low temperature CO oxidation.

Noble and transitional metals (Pt, Au, Cu and Ni) were loaded onto our CeO<sub>2</sub> supports with different shapes using an incipient wetness technique (impregnation method). To avoid complications arising from the presence of residual chlorine species, chlorine-free precursors such as Pt(NH<sub>3</sub>)<sub>4</sub>(NO<sub>3</sub>)<sub>2</sub>, Au(NO<sub>3</sub>)<sub>2</sub>, Cu(NO<sub>3</sub>)<sub>2</sub> or Ni(NO<sub>3</sub>)<sub>2</sub>·6H<sub>2</sub>O were added to the support with constant mixing. After suitable drying, the material then was calcined in air at 400 °C and reduced under hydrogen at 400 °C to prepare metal-supported CeO<sub>2</sub> nanocatalysts.

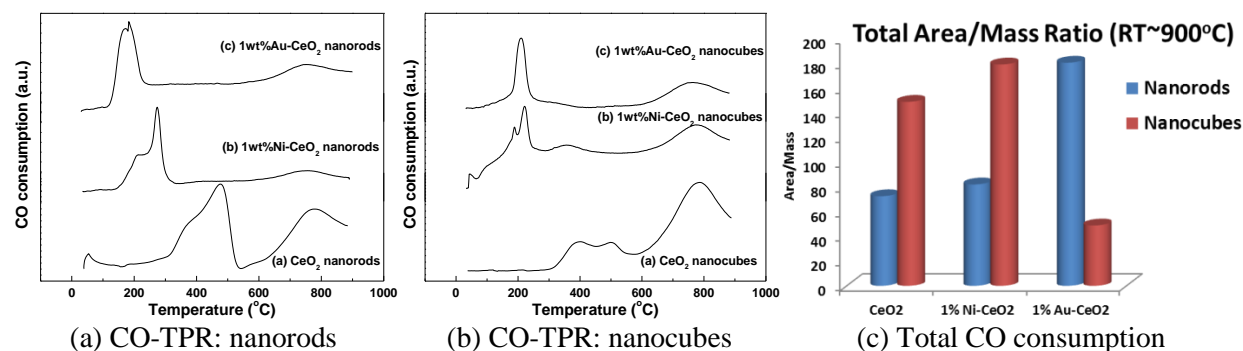


Figure 7. (a) and (b) CO-TPR comparison for CeO<sub>2</sub> nanorods, CeO<sub>2</sub> nanocubes, 1wt% Au/CeO<sub>2</sub> nanorods, 1wt% Ni/CeO<sub>2</sub> nanorods, 1wt% Au-CeO<sub>2</sub> nanocubes, and 1wt% Ni/CeO<sub>2</sub> nanocubes. (c) Quantitative CO consumption comparison from RT to 900°C for these six samples.

Figure 7 compares the shape effect of CeO<sub>2</sub> support on CO consumption of CeO<sub>2</sub> nanorods, CeO<sub>2</sub> nanocubes, and 1wt% Au-CeO<sub>2</sub>/1wt% Ni-CeO<sub>2</sub> nanorods and nanocubes. All metal-loaded samples show improved low-temperature activity, compared to pure CeO<sub>2</sub> nanorods and nanocubes. Surprisingly, when comparing the total CO consumption over the temperature range from room temperature to 900°C, Ni-CeO<sub>2</sub> nanocubes show higher CO consumption compared to Ni-CeO<sub>2</sub> nanorods, while Au-CeO<sub>2</sub> nanocubes show lower CO consumption compared to Au-CeO<sub>2</sub> nanorods. In other words, Ni and Au show different preference on the CeO<sub>2</sub> shape for low temperature CO oxidation. Ni prefers CeO<sub>2</sub> nanocubes to nanorods whereas Au prefers CeO<sub>2</sub> nanorods to nanocubes. This could be attributed to the interfacial anchoring effect of metals on different crystal planes on CeO<sub>2</sub> with different shapes, we investigated the atomic level interfacial structure and chemistry using HRTEM and EELS in details. Except for CO-TPR study, the CeO<sub>2</sub> and 1wt% metal (Pt, Au, Ni, Cu)/CeO<sub>2</sub> with different shapes were also examined using CO chemisorption on the Quantachrome iQ and Micrometrics 2920 to explore how much CO adsorbs as a function of temperature. Given that sufficient adsorption occurs, temperature programmed desorption (TPD) was used to determine

desorption temperature and desorption CO/CO<sub>2</sub> ratio. This information was used to determine the appropriate temperature for volumetric CO adsorption which then was carried out on the Quantachrome Autosorb iQ. CO adsorption was compared with BET measurements to determine the relative coverage of CO at the adsorption temperature. Figure 8 shows an example using the chemical reactor to compare the CO oxidation for the samples of 1wt% Au/CeO<sub>2</sub> nanorods and 1wt% Ni-CeO<sub>2</sub> nanocubes, and the TEM images were shown for the same two samples before and after metal loading (Figure 8 b and c). In the future, we expect that from this work we will be able to elucidate the effects of CeO<sub>2</sub> nanoparticle shape on catalytic activity of noble and transition metal nanoparticles, which will in turn be used to re-evaluate and guide our work on experimental optimization of CeO<sub>2</sub> morphology and size control.

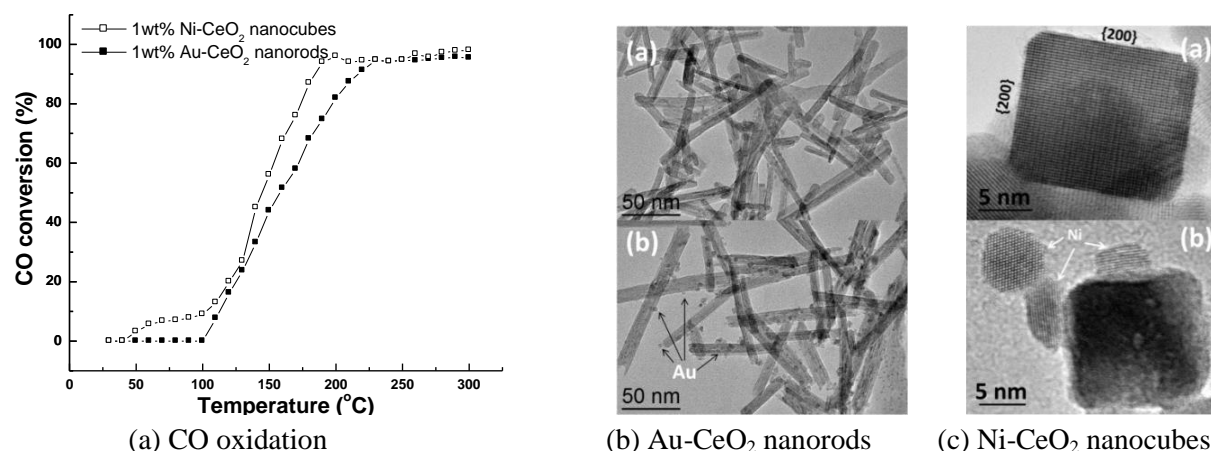


Figure 8. (a) CO oxidation over 1wt% Au/CeO<sub>2</sub> nanorods and 1wt% Ni-CeO<sub>2</sub> nanocubes. TEM images of 1wt% Au/CeO<sub>2</sub> nanorods (b) and 1wt% Ni-CeO<sub>2</sub> nanocubes (c) before and after metal loading.

### 3. Listing of Journal Publications and Conference Presentation Resulting from This Grant

- R. Wang, R. Dangerfield, Seed-mediated hydrothermal synthesis of shape-controlled CeO<sub>2</sub> nanocrystals, *RSC Advances*, 4(7): 3615-3620 (2014)
- R. Wang, S. Mutinda, Minghao Fang, One-pot synthesis and high temperature thermal stability in Ce<sub>x</sub>Zr<sub>1-x</sub>O<sub>2</sub> nanocrystals, *RSC Advances*, 3(42): 19508-19514 (2013)
- R. Dangerfield, D. Li, R. Wang, Low-temperature CO conversion on 1wt%Pt/CeO<sub>2</sub> nanocrystals, *Microsc Microanal* 19(Suppl 2): 1700-1701 (2013)
- Y. Xue, D. Yu, L. Dai, R. Wang, D. Li, A. Roy, F. Lu, H. Chen, Y. Liu, J. Qu, Three-dimensional B, N-doped graphene foam as metal-free catalysts for oxygen reduction reaction, *Phys. Chem. Chem. Phys.*, 15: 12220-12226 (2013)
- Y. Xue, J. Liu, H. Chen, R. Wang, D. Li, J. Qu, L. Dai, Nitrogen-doped graphene foams as metal-free counter electrodes in high-performance dye-sensitized solar cells, *Angew. Chem. Int. Ed.*, 51: 1214-12127 (2012) (Journal Cover)
- R. Wang, V. Sama, D. Li, S.I. Mutinda, Hydrothermal synthesis of rare-earth oxide nanocatalysts for automotive exhaust clean-up, *Advanced Materials Research*, 512-515: 1624-1629 (2012)

- R. Wang, S.I. Mutinda, D. Li, Size/shape-controlled synthesis and low-temperature reactivity of ceria, **Microsc Microanal** 18(Suppl 2): 1394-1395 (2012)
- R. Wang, M. Fang, Improved low-temperature reducibility in ceria zirconia nanoparticles by redox treatment, **J. Mater. Chem.**, 22: 1770-1773 (2012)
- R. Dangerfield, D. Li, R. Wang, Low-Temperature CO Conversion on 1wt%Pt/CeO<sub>2</sub> Nanocubes, **Microscopy & Microanalysis 2013**, Indianapolis, Indiana USA, August 4-8, 2013
- R. Dangerfield, R. Wang, Shape/Size-Reactivity Correlation Study in CeO<sub>2</sub> Nanocrystals, **23<sup>rd</sup> North America Catalysis Society Meeting**, Louisville, Kentucky USA, June 2-7, 2013
- (**Best Undergraduate Student Poster Award**) R. Dangerfield, R. Wang, Hydrothermal Synthesis and Reactivity Characterization of Ceria Nanoparticles, **American Chemical Society –The Penn Ohio Border Section Award Banquet**, Westminster College, New Wilmington, PA USA, April 19, 2013
- V. Sama, R. Wang, Synthesis and Characterization of CeO<sub>2</sub>-TiO<sub>2</sub> Nanotubes, **YSU Quest 2013**, Youngstown, Ohio USA, April 2, 2013
- R. Dangerfield, R. Wang, Hydrothermal Synthesis and Reactivity Characterization of Ceria Nanoparticles, **YSU Quest 2013**, Youngstown, Ohio USA, April 2, 2013

#### 4. References

Washes, I.E. *Catal. Today* **1996**, 27(3–4), 437-455.

Cuenya, B.R. *Thin Solid Films* **2010**, 518, 3127-3150.

Datye, A.K.; Logan, A.D.; Long, N.J. *J. Catal.* **1988**, 109(1), 76-88.

Flytzani-Stephanopoulos, M.; Gates, B.C. *Annu. Rev. Chem. Biomol. Eng.* **2012**, 3, 545-574

Gorte, R.J. *AIChE Journal* **2010**, 56, 1126-1135.

Lin, K.S.; Chowdhury, S. *Int. J. Mol. Sci.* **2010**, 11, 3226-3251

Yuan, Q.; Duan, H.H.; Li, L.L.; Sun, L.D.; Zhang, Y.W.; Yan, C.H. *J. Colloid Interface Sci.* **2009**, 335, 151-167